Publications of the Astronomical Society of the Pacific, **118**: 572–579, 2006 April

An Internet Database of Ultraviolet Continuum Light Curves for Seyfert Galaxies

Jay P. Dunn,[1] Brian Jackson,[2] Rajesh P. Deo,[1] Chris Farrington,[1] Varendra Das,[1] and D. Michael Crenshaw[1]
Received 2005 October 17; accepted 2006 January 4; published 2006 April 11

ABSTRACT. Using the Multimission Archive at STScI (MAST), we have extracted spectra and determined continuum light curves for 175 Seyfert galaxies that have been observed with the *International Ultraviolet Explorer* and the Faint Object Spectrograph on the *Hubble Space Telescope*. To obtain the light curves as a function of Julian Date, we used fixed bins in the object's rest frame and measured small regions (between 30 and 60 Å) of each spectrum's continuum flux in the range 1150 to 3200 Å. We provide access to the UV light curves and other basic information about the observations in tabular and graphical form via the Internet at http://www.chara.gsu.edu/PEGA/IUE.

1. INTRODUCTION

Seyfert galaxies harbor active galactic nuclei (AGNs) with typical redshifts $z \lesssim 0.1$ and moderate luminosities that vary over a range of timescales from days to years and over a factor of ∼10 in amplitude. AGNs have supermassive black holes consuming nearby gas and stars; the accretion disk surrounding the black hole is presumably the source for their high apparent luminosity and continuum variability. Seyfert galaxies are classified as types 1 and 2. Seyfert 1 galaxies have narrow (∼500 km s^{-1} FWHM) forbidden and permitted emission lines and broad (>1000 km FWHM) permitted lines, while Seyfert 2's have only narrow permitted and forbidden emission lines (Khachikian & Weedman 1974). Ultraviolet spectra of Seyfert galaxies are notable for their strong continuum variability, which is not as pronounced in the visual regime (e.g., NGC 4151; Kaspi et al. 1996).

The *International Ultraviolet Explorer* (*IUE*) began monitoring AGNs in 1978 and collected a large number of UV spectra through 1995, while the Faint Object Spectrograph (FOS) on board the *Hubble Space Telescope* collected spectra from 1990 through 1997. Although the origin of the UV continuum is still elusive, the current belief is that it is radiated from the accretion disk. Comparisons of variability in the UV with other regions of the spectrum place important constraints on the physics involved (e.g., Nandra & Papadakis 2001). Thus, it is important to have a comprehensive and uniform database of UV light curves for comparison with continuum observations at other wavelengths.

From the massive collection of *IUE* and FOS spectra, we have compiled continuum light curves and created a database that is Internet accessible. Our list of targets includes any object that has been designated as a Seyfert galaxy by the observing astronomer for any observation with either *IUE* or the *Hubble Space Telescope* (*HST*). In addition, we have limited the selection list by redshift, including only objects with a redshift $z < 0.2$. Our database is the first effort to make AGN UV light curves readily available via the World Wide Web. The only previous effort was an atlas of *IUE* spectra of Seyfert galaxies observed prior to 1991 January 1 (Courvoisier & Paltani 1992). The database we have created is inclusive of all *IUE* and FOS spectra through their final years and has the capability to receive further observations provided by sources such as the Goddard High Resolution Spectrograph (GHRS), the Space Telescope Imaging Spectrograph (STIS), and the Hopkins Ultraviolet Telescope (HUT). This information should be helpful for a number of studies, including those that require (1) the history of the UV continuum variations for an individual Seyfert galaxy, (2) a comparison of UV fluxes with measurements in other regimes of the electromagnetic spectrum for any given epoch, and (3) detailed statistical analyses (e.g., cross-correlation and structure functions) of the UV continuum properties of AGNs.

2. OBSERVATIONS

2.1. *International Ultraviolet Explorer*

IUE was launched on 1978 January 26 and operated successfully until 1996 September 30, when it was decommissioned. *IUE* had the capability of performing spectroscopy at two different resolutions. The high-resolution mode operated at a spectral resolution of 0.1–0.3 Å (FWHM), while the low-resolution mode performed at 6–7 Å (FWHM). *IUE* had two apertures available for spectroscopy: large (10″ × 20″) and small (3″ in diameter). Due to the faintness of Seyfert galaxies, the high-resolution mode is unsuitable for continuum studies. Observations through the small aperture are unsuitable for absolute photometry, due to the large (∼50%) and variable light loss. Thus, we used only large-aperture, low-dispersion spectra

[1] Department of Physics and Astronomy, Georgia State University, Atlanta, GA 30303-4106; dunn@chara.gsu.edu.
[2] Lunar and Planetary Laboratory, University of Arizona, Tucson, AZ 85721-0092.

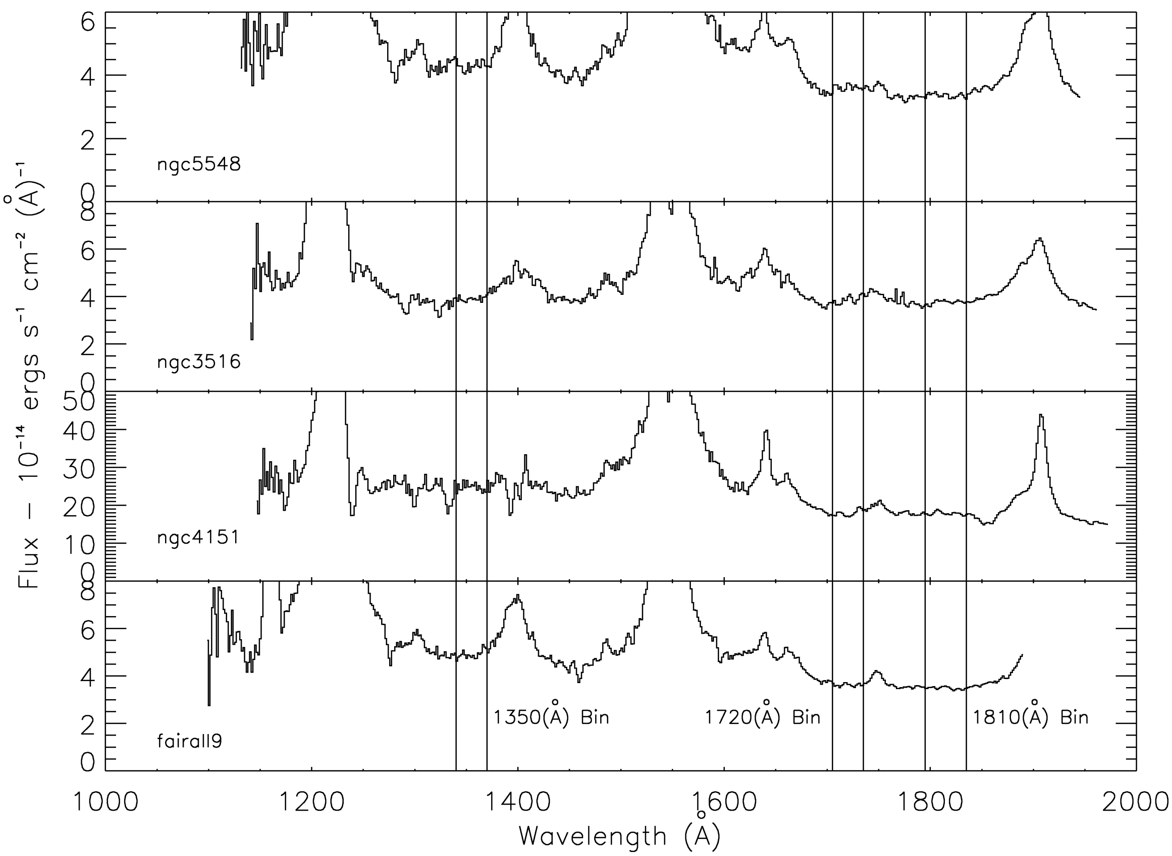

FIG. 1.—Plots of *IUE* SWP spectra for four frequently observed Seyfert galaxies in each object's rest frame to determine the best locations and sizes for bin measurements. These are average spectra from all of the good-quality spectra provided by MAST. The bin locations and widths used for determining the light curves are shown.

for the light curves. *IUE* utilized a total of four cameras: the long-wavelength prime (LWP) and redundant (LWR) cameras and the short-wavelength prime (SWP) and redundant (SWR) cameras, which operated at 1850–3200 and 1150–2000 Å, respectively. The SWR camera was only used for a handful of observations early on, and no useful data on Seyfert galaxies were obtained. Both the LWP and LWR cameras were used to make observations over the lifetime of *IUE*. During *IUE*'s early life, the LWR camera dominated the observing; during the later years, the LWP camera become the dominant camera, due to a flare that developed in the LWR.[3]

2.2. Faint Object Spectrograph

The FOS was one of the initial spectrographs installed on the *HST*, which was launched in 1990. It remained on board *Hubble* until 1997. There are two versions of the FOS data, pre-COSTAR and post-COSTAR, corresponding to data obtained before and after the optics were repaired on *HST* in 1994 January. The optics correction caused a slight change in the aperture sizes, but there were no major effects on the quality of the data. We chose to use data from all apertures, since aperture corrections for the FOS are highly reliable. The FOS had two spectral resolutions available: high ($\lambda/\Delta\lambda \sim 1300$) and low ($\lambda/\Delta\lambda \sim 250$). For our sample, we chose to use the high-resolution grating, due to the short exposure times and resulting poor signal-to-noise ratio in the low-resolution spectra. Although the FOS gratings covered both the UV and visible regimes, we chose to use only the UV data, from gratings G130H, G190H, and G270H, with wavelength ranges spanning 1000–1700, 1700–2200, and 2200–3000 Å, respectively.[4]

3. DATA REDUCTION AND ANALYSIS

For our purposes, every available spectrum was obtained using the MAST (Multimission Archive at STScI) interface. The first objective was to create a single averaged spectrum

[3] See http://archive.stsci.edu/iue for detailed information on the *IUE* telescope and instruments.

[4] See http://www.stecf.org/poa/FOS for detailed information on the FOS.

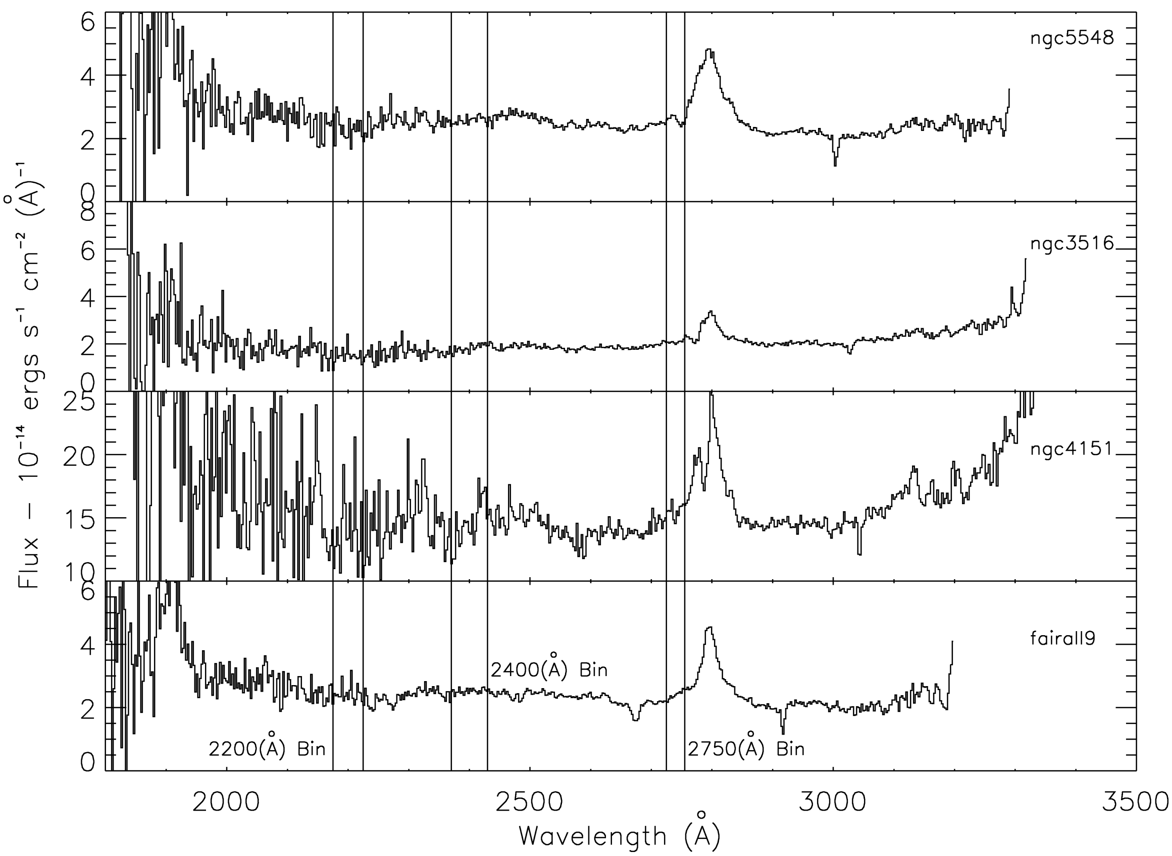

FIG. 2.—Plot of average LWP spectra for the same four Seyfert galaxies as in Fig. 1. Bin locations and widths are indicated.

per AGN from a short list of viable candidates, to identify suitable continuum regions. We chose NGC 5548, NGC 4151, Fairall 9, and Mrk 509, primarily due to their numerous *IUE* observations (367, 984, 233, and 97 observations, respectively). To view the common emission lines, the average spectra were deredshifted and plotted together, as shown in Figures 1 and 2. We determined from the figures where continuum flux measurements were possible with little chance of an emission or absorption line altering the flux measurements. The best locations for the SWP camera measurements fell at 1355, 1720, and 1810 Å, with bin sizes of 30, 30, and 50 Å, whereas the LWP/LWR camera bins fell at 2200, 2400, and 2740 Å, with bin sizes of 50, 60, and 30 Å, all in the rest frame of the galaxy. Note that fluxes in the 2200 Å bin are rather noisy compared to the other bins, due to the low sensitivities of the cameras in this region.

Our next step was to remove flawed spectra from the sample. Several reasons arose for eliminating certain *IUE* spectra from the light-curve list. One such reason was overexposure. The *IUE* cameras had a limited dynamic range such that the raw counts (in data numbers, DN) could not exceed the value of 255. Although in most cases only the emission lines were overexposed, we decided to be cautious and not use overexposed images for our continuum measurements, due to possible nonlinearity effects in spectra with large differences in exposure level (Nichols & Linsky 1996 and references therein). However, the data are still in MAST and are readily available for reduction and addition to the light curves we have provided. Another problem that appeared was heavy background noise during periods of *IUE*'s orbit. As *IUE* orbited the Earth, it would daily fall into the Van Allen belts. These events would send background counts up to high levels, thereby making the continuum fluxes very noisy. Low to moderate background values turned out to be between 50 and 100 DN; values above 100 DN were considered high, and those above 200 DN were unusable. To set a standard limit, we have omitted any spectra with background >100 DN. During *IUE*'s later years, sunlight leaked into the telescope and added an extended source of light at wavelengths longer than 2500 Å. All spectra observed after 1990 that exhibited an unusually large increase in continuum slope in the LWR and LWP images due to this effect were excluded from our light curves. Other less prominent events affected the *IUE* spectra but were either rare or did not affect the continuum flux. On

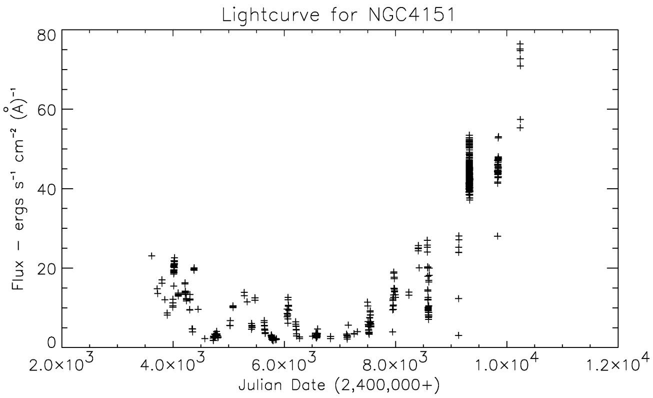

FIG. 3.—Example light curve plot of the 1355 Å bin for NGC 4151. This particular light curve shows an excellent example of large-scale changes in flux over significant periods of time.

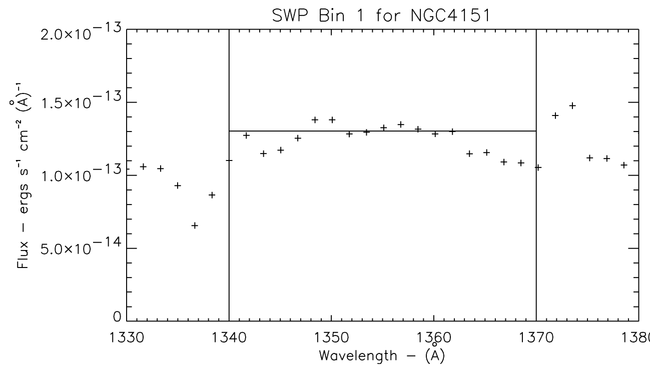

FIG. 5.—Example of the 1355 Å bin with the SWP camera for NGC 4151, zoomed-in to show the average flux within the bin. The points are the sampled fluxes from *IUE*, and only the points inside of the bin are measured. The error calculated is the standard deviation of the observed points from that average flux.

our Web site, we provide for each object a list of spectra that were removed from our measurements, along with a key of explanations of what events occurred to exclude the spectra.

Once we established a quality standard, we shifted our predetermined wavelength bins by $1 + z$ to measure the fluxes in the object's frame. For example, in NGC 4151 ($z = 0.0033$) the SWP bin positions shifted to 1359, 1725, and 1816 Å. When redshifting a bin near the edge of a spectrum, the 1810 Å bin in the SWP and the 2740 Å bin in the LWP camera would occasionally fall off the spectrum and yield a null result. This occurence is the reason for a redshift limit of $z < 0.2$ in our selection list.

As discussed above, the FOS had three fixed grating ranges available. This meant that unlike the *IUE* data set, there was typically one bin in the G130H (the 1355 Å bin), three bins in the G190H (the 1720, 1810, and 2200 Å bins), and two bins in the G270H (the 2400 and 2740 Å bins) spectra. When examining light curves composed of data from each source, it should be noted that the quality of spectra for measurements in the 1355 and 1720 Å bins on the FOS could be vastly different, yet with *IUE* observations, these two bins were obtained at the same time and with the same camera and were thus less likely to contain deviations from one another.

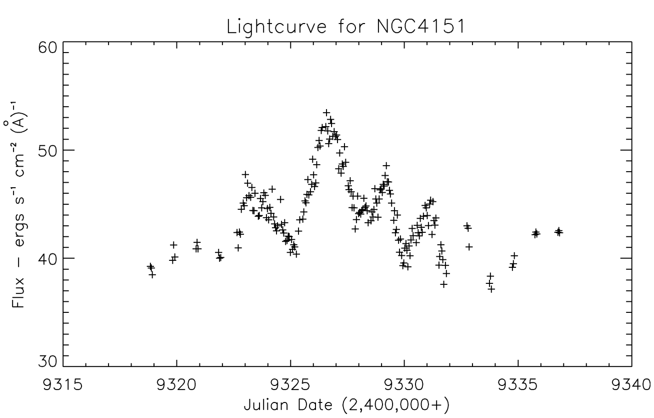

FIG. 4.—Zoomed-in version of Fig. 3. Error bars are not shown, for clarity.

Once the measurements were made, we plotted the average flux in each bin versus the Julian Date of the midpoint of each exposure, calculated from the start time of the observation and the exposure length, which were taken from the file header provided by MAST. In order to extend the time span in which objects were monitored, we combined the light curves from the FOS and *IUE*. An example of these results is displayed for NGC 4151 in Figure 3, along with a zoomed-in section in Figure 4. In these light curves, it is obvious that over long time frames (years) the flux can change by a factor of 10, as previously mentioned. In Figure 4, it can be seen that small flux changes occurred over the course of 3 days' time in the intense monitoring campaign during this time period. This is one of the few occasions in which the observations did not undersample the continuum variations (Crenshaw et al. 1996).

Continuum fluxes at the level of $\sim 2 \times 10^{-15}$ ergs s^{-1} cm^{-2} $Å^{-1}$ or smaller are unreliable, due to camera artifacts and uncertain background levels in the *IUE* cameras (Crenshaw et al. 1990). Note that extended continuum sources, such as starbursts or scattering regions often found in Seyfert 2 galaxies, could show apparent flux variability due to the different aperture sizes used by *IUE* and the FOS.

4. ERROR ANALYSIS

In order to determine the uncertainties in the *IUE* fluxes, we began by establishing the average of the continuum in each bin, illustrated by the horizontal line in Figure 5, and then

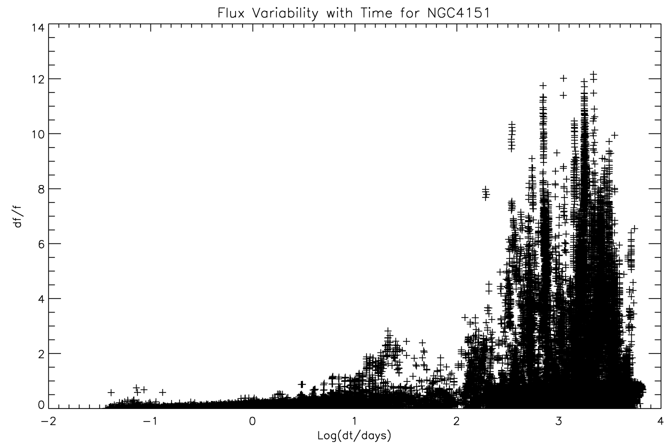

FIG. 6.—Plot of the change in flux vs. the change in time for NGC 4151.

measured the standard deviation σ of the points within the designated bins. This method for *IUE* error determination is known to overestimate the uncertainties (Clavel et al. 1991). Because the *IUE* cameras were not photon counters and the spectra were highly oversampled, there are approximately four spectral points per wavelength resolution element.

For our measurements, we concluded that a method of adjusting the error bars that is similar to that given in Clavel et al. (1991) is optimal. Previous studies have shown that on timescales of less than 1–2 days, the UV continuum variations in Seyfert galaxies are small (see Fig. 4). Thus, any apparent continuum variability exhibited on very short timescales in the *IUE* data is likely dominated by photon and/or instrument noise. To test this notion, we performed combinatorics of all points in light curves for several objects that contained at least tens of observations. We determined the fractional change in flux ($\delta f/f = |f_1 - f_2|/f_1$) and time ($\delta t$) between every two points (it should be noted that this is similar to a structure function method).

Figure 6 shows a plot of $\delta f/f$ against δt for each pair of points in Figure 3. As expected, as the time interval grows, the maximum change in flux grows. The leveling off of points on time intervals of less than ~1 day confirms that there is no significant excess variability above the noise level (with the exception of a few points) on short timescales.

We took measurements of the data points contained within a rectangle between log δt(days) of -1.5 and -0.5 and between $\delta f/f$ of 0.0 and 0.15 in Figure 6 to characterize the noise. We define the reproducibility R as the average of the fractional variations in the time bin. Here R represents an upper limit to the flux uncertainty (on average), since we cannot rule out the possibility of small variations on these short timescales. The mean measured error $E_{\rm mean}$ is given by the average of all of the uncertainties for each of the measured fluxes within the given bin (σ) in this time interval. The overestimation of the error is given by the ratio of the mean measured error $E_{\rm mean}$ and the reproducibility R. Thus, if we divide our individual σ by this ratio, we obtain an estimate of the noise in each measurement, but scaled appropriately.

We repeated the above procedure for a number of well-observed Seyfert galaxies. In Tables 1–3, we present the necessary data to determine the overestimation of the error for each camera. We imposed the limits log $\rm JD_{max}$ and log $\rm Flux_{max}$ on the region of the plot of $\delta f/f$ versus log δt to determine the reproducibility. The ratio is the average error $E_{\rm mean}$ divided by the reproducibility R, or in other words, the factor by which the original errors have been overestimated. The reciprocal of the ratio averaged over all objects gives the final scaling factor for the original errors. The average ratios

TABLE 1
ERROR ANALYSIS OF *IUE* DATA FOR SEYFERT GALAXIES: SWP

Object	log $\rm JD_{max}$	log $\rm Flux_{max}$	R[a]	$E_{\rm mean}$	Ratio
NGC 4151	−0.50	0.15	0.032	0.067	2.06
NGC 7469	−0.50	0.20	0.045	0.076	1.67
NGC 3783	0.00	0.30	0.054	0.073	1.36
NGC 3516	0.20	0.15	0.046	0.081	1.76
NGC 5548	0.25	0.15	0.048	0.085	1.78
Fairall 9	0.25	0.15	0.057	0.099	1.74
3C 390.3	1.50	0.50	0.222	0.272	1.22
Mrk 509	0.75	0.20	0.040	0.080	1.99
Mrk 335	1.00	0.30	0.091	0.099	1.09
NGC 4593	1.00	0.50	0.129	0.115	0.89
RX J2304.7−0841	1.50	0.50	0.114	0.150	1.32

[a] Reproducibility.

TABLE 2
ERROR ANALYSIS OF *IUE* DATA FOR SEYFERT GALAXIES: LWR

Object	log $\rm JD_{max}$	log $\rm Flux_{max}$	R[a]	$E_{\rm mean}$	Ratio
NGC 4151	−0.50	0.15	0.030	0.103	3.43
NGC 7469	1.50	0.20	0.054	0.082	1.52
NGC 3783	0.50	0.15	0.072	0.109	1.51
NGC 3516	2.30	0.20	0.078	0.102	1.31
NGC 5548	1.50	0.15	0.064	0.164	2.56
Fairall 9	1.00	0.10	0.034	0.099	2.91
3C 390.3	2.50	0.20	0.073	0.214	2.93
RX J2304.7−0841	2.00	0.20	0.037	0.111	3.00

[a] Reproducibility.

TABLE 3
ERROR ANALYSIS OF *IUE* DATA FOR SEYFERT GALAXIES: LWP

Object	log $\rm JD_{max}$	log $\rm Flux_{max}$	R[a]	$E_{\rm mean}$	Ratio
NGC 4151	−1.00	0.15	0.028	0.050	1.78
NGC 3783	0.00	0.15	0.032	0.043	1.34
NGC 5548	0.50	0.25	0.064	0.088	1.38
Fairall 9	0.00	1.00	0.028	0.058	2.07
3C 390.3	1.70	1.20	0.056	0.120	2.14
Mrk 335	1.00	0.10	0.049	0.087	1.78

[a] Reproducibility.

Light Curve Database: Object list sorted by RA (J2000)

Object	Redshift	Right Ascention	Declination	Data Points	Redshifted Bin Wavelength
MRK1501	0.08934	00 10 31.0	+10 58 29.5	45	1476 1873 1971 2396 2614 2984
ESO242-8	0.05604	00 25 01.3	-45 29 55.3	3	1430 1816 1911
WPV007	0.02882	00 39 15.6	-51 17 03.0	16	1394 1769 1862 2263 2469 2818
IRAS00392-7930	0.03002	00 40 45.2	-79 14 24.3	6	1395 1771 1864 2266 2472 2822
MRK348	0.01503	00 48 47.1	+31 57 25.1	8	1375 1745 1837 2233 2436 2781
UGC00524	0.03596	00 51 35.0	+29 24 04.5	3	2279 2486 2838
IZW1	0.00537	00 53 34.9	+12 41 36.2	39	1362 1729 1819 2211 2412 2754
TONS180	0.06198	00 57 19.9	-22 22 59.1	27	1438 1826 1922 2336 2548 2909
MRK352	0.01486	00 59 53.3	+31 49 36.9	9	1375 1745 1836 2232 2435 2780
NGC0424	0.01166	01 11 27.7	-38 05 00.5	12	1370 1740 1831 2225 2427 2771
MRK1152	0.05271	01 13 50.1	-14 50 44.1	6	1426 1810 1905 2315 2526 2884
MRK975	0.04963	01 13 51.0	+13 16 18.2	6	1422 1805 1899
MRK1	0.01595	01 16 07.2	+33 05 22.4	8	1376 1747 1838 2235 2438 2783
MCT0117-2837	0.055	01 19 35.6	-28 21 31.0	3	1429 1814 1909
FAIRALL9	0.04702	01 23 45.8	-58 48 20.5	705	1418 1800 1895 2303 2512 2868
MRK359	0.01739	01 27 32.6	+19 10 45.8	21	1378 1749 1841 2238 2441 2787
MICH343	0.01722	01 36 00.2	+00 39 48.7	3	1378 1749 1841
MRK573	0.01726	01 43 57.8	+02 20 59.7	8	1378 1749 1841 2237 2441 2787
MCT0146-2813	0.12	01 48 22.3	-27 58 25.0	3	1517 1926 2027
MICH385	0.16301	01 59 50.2	+00 23 40.6	6	1575 2000 2105 2558 2791 3186
MRK1018	0.04244	02 06 16.0	-00 17 29.2	24	1412 1792 1886 2293 2501 2856
MRK590	0.02638	02 14 33.6	-00 46 00.1	6	1390 1765 1857 2258 2463 2812
NGC931	0.01665	02 28 14.5	+31 18 42.0	3	1377 1748 1840 2236 2439 2785

FIG. 7.—Sample image of Web site home page.

are 1.69 ± 0.34, 2.40 ± 0.77, and 1.75 ± 0.31 for the SWP, LWR, and LWP cameras, respectively. For the FOS data, in the few instances in which we have multiple observations of an object over short timescales, we see no evidence that the error bars require additional scaling.

5. DATABASE AND WEB SITE

We have created a Web site to make our UV light curves of Seyfert galaxies available to the community. Users can access our Web site at http://www.chara.gsu.edu/PEGA/IUE. We chose to create a MySQL database to store the data and have built our Web site with Perl CGI scripts. The opening page is a tabular list of the objects for which we have data, sorted by right ascension (see Fig. 7). It should be noted that right ascension and declination are provided in the J2000.0 epoch. Users can use their Web browser's "find" function to locate an object by name. The main page presents not only the list of objects and positions, but also their respective redshifts and a link to the light curve for each bin that was measured (the central position of the bin is given in the observed frame). For each link, we provide an on-the-fly light-curve generator (Fig. 8). The user is able to adjust the time frame or the flux range within the window to allow for a zoom. For each light curve, users can click on any point to access the observing information for that point. We also provide a link to the information for all observations in the bandpass, as well as the light curve data in tabular form (Julian Date [for observation start time], fluxes, and scaled uncertainties) for downloading, as shown in Figure 9. This list also gives the observations that were removed from the light curve, if any. From this page, users are also able to access previews of the original spectra on the MAST Web site. In the future, we hope to add

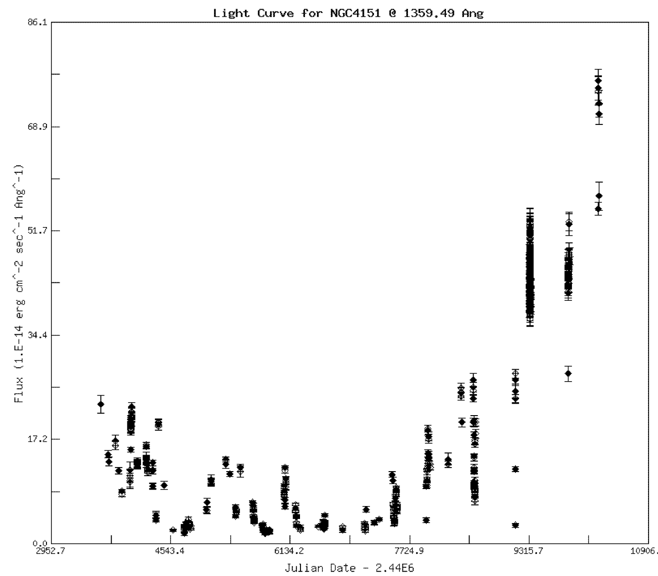

FIG. 8.—Sample image of the on-the-fly light-curve generator.

Light Curve Points for NGC4151 @ 1359.49 Ang

Back to Light Curve

MAST ID	Obs. Date	Obs. Julian Date	Disp./ Grating	Aperture	Right Ascention	Declination	Exposure	Instrument	Flux	Error
SWP01372	1978-04-16 23:18:00	3615.48	Low	Large	12 10 32.69	+39 24 21.57	2400.00	SWP	23.05	1.45
SWP02098	1978-07-24 22:24:00	3714.44	Low	Large	12 10 31.50	+39 24 18.44	1800.00	SWP	14.79	0.62
SWP02171	1978-08-02 02:08:00	3722.60	Low	Large	12 10 31.50	+39 24 10.52	1800.00	SWP	13.58	0.74
SWP03048	1978-10-19 17:25:00	3801.24	Low	Large	12 10 31.50	+39 24 18.44	1800.00	SWP	17.07	0.84
SWP03049	1978-10-19 18:34:00	3801.28	Low	Large	12 10 31.50	+39 24 18.44	1500.00	SWP	16.18	0.67
SWP03557	1978-12-09 11:46:00	3852.00	Low	Large	12 10 31.50	+39 24 12.68	1800.00	SWP	12.05	0.51
SWP03971	1979-01-21 13:15:00	3895.06	Low	Large	12 10 31.50	+39 24 18.44	1500.00	SWP	8.69	0.32
SWP03972	1979-01-21 15:22:00	3895.15	Low	Large	12 10 31.50	+39 24 18.44	1500.00	SWP	8.14	0.34
SWP05100	1979-05-03 05:14:00	3996.73	Low	Large	12 10 31.50	+39 24 18.44	1500.00	SWP	10.15	1.03
SWP05101	1979-05-03 06:25:00	3996.78	Low	Large	12 10 31.50	+39 24 18.44	1500.00	SWP	10.50	1.11
SWP05102	1979-05-03 07:26:00	3996.82	Low	Large	12 10 31.50	+39 24 18.44	1500.00	SWP	11.24	1.05

FIG. 9.—Sample of the light-curve information page.

points to the light curves from other UV spectrographs, such as GHRS, STIS, and HUT.

This research has made use of the NASA/IPAC Extragalactic Database (NED), which is operated by the Jet Propulsion Laboratory, California Institute of Technology, under contract with the National Aeronautics and Space Administration. All of the data presented in this paper were obtained from the Multimission Archive at the Space Telescope Science Institute (MAST). Support for MAST for non-*HST* data is provided by the NASA Office of Space Science through grant NAG 5-7584 and by other grants and contracts.

REFERENCES

Clavel, J., et al. 1991, ApJ, 366, 64
Courvoisier, T. J.-L., & Paltani, S. 1992, *IUE*-ULDA Access Guide No. 4 (ESA SP-1153A/B) (Noordwijk: ESA)
Crenshaw, D. M., Bruegman, O. W., & Norman, D. J. 1990, PASP, 102, 463
Crenshaw, D. M., et al. 1996, ApJ, 470, 322
Khachikian, E. Y., & Weedman, D. W. 1974, ApJ, 192, 581
Kaspi, S., et al. 1996, ApJ, 470, 336
Nandra, K., & Papadakis, I. E. 2001, ApJ, 554, 710
Nichols, J. S., & Linsky, J. L. 1996, AJ, 111, 517